"Thermic End-Fire" Interstitial Applicator for Microwave Hyperthermia

Graziano Cerri, Roberto De Leo, and Valter Mariani Primiani

Abstract—**This paper presents the analysis of a "thermic end-fire" interstitial applicator for microwave hyperthermia, i.e., an applicator that performs a tip localized heating of the surrounding lossy medium. The antenna consists of a shorted coaxial cable with an annular radiating aperture at the end. The analytical approach is based on the equivalence principle, which leads to an integral equation for the equivalent magnetic current distribution on the aperture; solution is achieved by the Method of Moments. All theoretical results have been compared to experimental ones showing a good agreement in a wide frequency range.**

I. Introduction

INTERSTITIAL applicators for microwave hyperthermia treatments have gained a large interest because they offer some advantages with respect to superficial applicators. Despite the disadvantage of being an invasive technique, it is well known that interstitial hyperthermia is very effective to heat deep-seated tumors, realizing an extremely localized temperature increase with a minimum risk of damage to surrounding healthy tissues; moreover, the applicators have a small size and are easy to fabricate. From an electrical point of view, a good matching to the source can be obtained; radiation pattern, and consequently temperature distribution, can be easily controlled when these applicators are used in array configuration; the same antennas can also be used for temperature monitoring during the treatment.

The behavior of this antenna, embedded in a biological tissue, has been extensively investigated, and many papers are available in the literature.

Clinical studies have well assessed the performances of interstitial hyperthermia, often used in combination with interstitial radiotherapy (see, for example, [1]–[6]), and have shown the possibility of temperature measurements from sensors within interstitial applicators [7].

At the same time, theoretical models have been developed in order to characterize the electric behavior of the interstitial antenna; the evaluation of the current distribution on the dipole, and the electric field in the surrounding dissipative medium can be found in [8]–[10]. Subsequently, many interstitial applicators have been designed, investigated, and optimized [11]–[15].

Arrays of interstitial antennas have also been analyzed because they perform, for some combinations of the feeding currents, a uniform heating of large tumors [16]–[21].

Manuscript received April 6, 1992; revised October 30, 1992.

The authors are with the Dipartimento di Elettronica e Automatica, Università di Ancona, Via Brecce Bianche, 60131 Ancona, Italy.

IEEE Log Number 9209329.

While the above-mentioned papers deal with applicators radiating in a plane perpendicular to the axis of the antenna, a new interstitial microwave antenna has recently been designed to provide enhanced tip heating, consisting of a balun-fed, folded dipole [22], [23]; it has been successfully tested for vascular interventions in dogs [24].

In the present paper, a different interstitial applicator, but with similar thermic characteristics, has been theoretically and experimentally analyzed; it consists of a shorted coaxial cable with an annular radiating slot placed very close to the end of the cable.

This structure exhibits a localized heating at the tip of the applicator, and because of this characteristic it has been named "thermic end-fire" applicator, meaning that the thermic pattern shows a lobe along the axis of the cable beyond and around its end.

This applicator has been adopted after an experimental study of several coaxial radiating terminations [25]. In fact, this antenna realizes the best compromise between mechanical and electrical requirements. The applicator has to be very thin, but its mechanical strength must be compatible with clinical applications; moreover, it has to be well matched to secure a sufficient power delivered into the tissues.

The analytical model allows us to set up an equation for the electric field on the radiating slot. The approach is based on the equivalence principle, and the solution is achieved by means of a simplified form of the Method of Moments.

From the knowledge of the electric field on the aperture, it is possible to evaluate the electric behavior of the applicator in terms of return loss, and its thermic characteristics in terms of temperature pattern; this is essential in clinical practice, to be able to asses the power delivered into the tissue to reach a prefixed temperature distribution.

II. Formulation of the Problem

Fig. 1 shows the geometry of the problem: a small radiating slot has been obtained in $z_1 \leq z \leq z_2$ by removing all around the external conductor of a coaxial cable shorted at $z = z_{sc}$; the inner and the outer radius of the conductors are r_i and r_o, respectively, and the relative permittivity of the dielectric filling the cable is ε_d; the structure is embedded in a lossy, homogeneous material of complex relative permittivity $\varepsilon = \varepsilon' - j\varepsilon''$.

The analytical approach is based on the equivalence principle: a conducting surface S is placed over the radiating aperture, and a proper distribution of equivalent magnetic current is considered on S (Fig. 2), inside the cable (M^a)

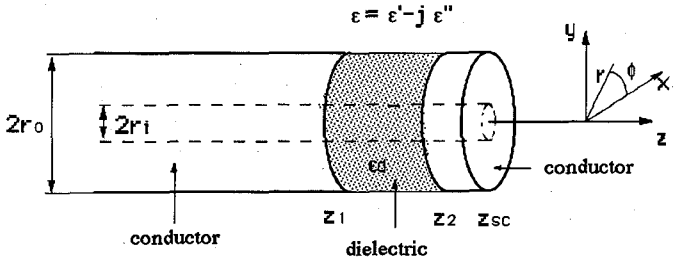

Fig. 1. Geometry of the problem.

and outside the cable (M^b):

$$M^a = a_r \times E = -M \tag{1a}$$

$$M^b = E \times a_r = M \tag{1b}$$

E being the electric field on the aperture, and a_r the radial unit vector of a cylindrical coordinate system (shown in Fig. 1), normal to the surface S.

Continuity of the total tangential magnetic field allows us to achieve an equation for the unknown distribution M

$$H_T^a = H_T^b . \tag{2}$$

By use of the equivalence principle, the original problem is divided in two simpler problems: the evaluation of the magnetic field inside the cable (region "a") and in the biological medium (region "b") separately.

$$H_T^a = H_t^i + H_t^a(-M) = H_t^i - H_t^a(M) \tag{3a}$$

$$H_T^b = H_t^b(M) . \tag{3b}$$

In region "a," the field is due to the source (H_t^i) and to $-M(H_t^a(-M))$; in region "b," it is due to M only ($H_t^b(M)$). Substituting (3) in (2), the sought equation for M is obtained

$$H_t^a(M) + H_t^b(M) = H_t^i . \tag{4}$$

The solution is achieved by use of the Method of Moments [26], so (4) is changed into a matrix equation

$$([Y^a] + [Y^b])[V] = [I] \tag{5}$$

where

$$Y_{mn}^{a/b} = \left\langle W_m, H_t^{a/b}(f_n) \right\rangle \tag{6}$$

$$I_m = \langle W_m, H_t^i \rangle \tag{7}$$

$$V_m = \text{unknown term vector} \tag{8}$$

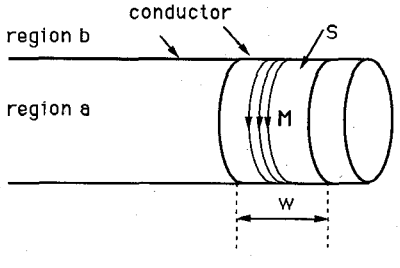

Fig. 2. Application of the equivalence principle.

f_n, W_m being the nth expansion function and the mth test function, respectively; the inner product is defined as integration over S

$$\langle A, B \rangle = \int_S A \cdot B \, dS . \tag{9}$$

Assuming $\partial/\partial\phi = 0$ (cylindrical symmetry) and slot width $w = (z_2 - z_1) \ll \lambda$, only the E_z component of the electric field on S is considered. From (1), the magnetic current is given by

$$M = M_\phi(z) a_\phi = \begin{cases} V_o f(z) a_\phi & \text{on } S \\ 0 & \text{elsewhere} \end{cases} \tag{10}$$

where just one expansion function $f(z)$ is used to describe the magnetic current; so the linear system (5) reduces to one equation, and the unknown amplitude V_o is simply given by

$$V_o = \frac{I}{Y^a + Y^b} . \tag{11}$$

If a pulse function is chosen as test function

$$W = \begin{cases} 1 a_\phi & \text{on } S \\ 0 & \text{elsewhere} \end{cases} \tag{12}$$

from (6) and (7), omitting the unnecessary subscripts,

$$Y^a + Y^b = \int_S H_\phi^a(r_o, z, f(z)) \, dS + \int_S H_\phi^b(r_o, z, f(z)) \, dS \tag{13a}$$

$$I = \int_S H_\phi^i(r_o, z) \, dS . \tag{13b}$$

III. Source Term I

The excitation is represented by a TEM mode of unit amplitude: the wave impinges on the short and is totally reflected (Fig. 3)

$$E_r^i(r, z) = \frac{1}{r} e^{-j\beta z} + \Gamma_o \frac{1}{r} e^{j\beta z} \tag{14a}$$

$$H_\phi^i(r, z) = \frac{1}{r\eta} e^{-j\beta z} - \Gamma_o \frac{1}{r\eta} e^{j\beta z} \tag{14b}$$

where

$$\beta = \omega\sqrt{\mu_o \varepsilon_o \varepsilon_d}; \qquad \eta = \sqrt{\frac{\mu_o}{\varepsilon_o \varepsilon_d}} \tag{15a}$$

$$\Gamma_o = -e^{-2j\beta z_{sc}} . \tag{15b}$$

The source element I in (13b) is easily evaluated

$$I = \frac{4\pi}{\omega\mu_o} e^{-j\beta z_{sc}} [\sin\beta(z_{sc} - z_1) - \sin\beta(z_{sc} - z_2)] . \tag{16}$$

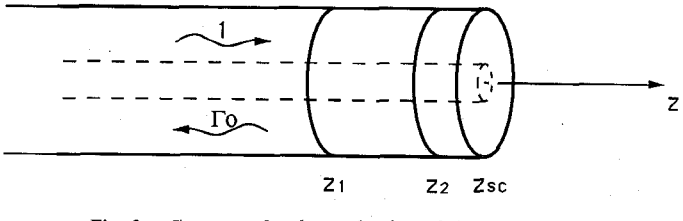

Fig. 3. Geometry for the evaluation of the source term.

IV. Admittance Term Y^a

According to (13a), the magnetic field H_ϕ^a inside the cable, excited by the magnetic current, may be expressed as the summation of TEM and TM modes; the cable dimensions allow propagation of the TEM mode only (all TM modes are below cutoff); moreover, the considered source does not excite TE modes.

As shown in Fig. 4, the field generated by M^a consists of a forward wave (E^+, H^+), which reflects on the short circuit (E^R, H^R) and a backward wave (E^-, H^-). In particular, the TEM ϕ-directed magnetic field is

$$H^+_{\phi\mathrm{TEM}}(r,z) = \frac{C_o^+}{r\eta}\, e^{-j\beta z} \tag{17a}$$

$$H^-_{\phi\mathrm{TEM}}(r,z) = -\frac{C_o^-}{r\eta}\, e^{j\beta z} \tag{17b}$$

$$H^R_{\phi\mathrm{TEM}}(r,z) = -\Gamma_o \frac{C_o^+}{r\eta}\, e^{j\beta z} \tag{17c}$$

Lorentz' reciprocity theorem allows the evaluation of the modal amplitudes

$$C_o^\pm = \pm \frac{V_o}{2\ln\left(\frac{r_o}{r_i}\right)} \int_{z_1}^{z_2} e^{\pm j\beta z} f(z)\, dz \tag{18}$$

so that the fields in the two sections of the cable, before and after the magnetic source, are completely determined

$$H_{\phi\mathrm{TEM}}(r,z) = -\frac{e^{j\beta z}}{r\eta}\left[C_o^- + \Gamma_o C_o^+\right] \qquad z \le z_1 \tag{19a}$$

$$H_{\phi\mathrm{TEM}}(r,z) = C_o^+ \frac{e^{-j\beta z_{sc}}}{r\eta}\, 2\cos\beta(z_{sc}-z) \qquad z_2 \le z \le z_{sc}\,. \tag{19b}$$

Using the same technique, the field of higher order modes can be evaluated

$$H_{\phi\mathrm{TM}}(r,z) = j\omega\varepsilon_o\varepsilon_d \sum_{n=1}^{\infty} \frac{S_1(k_{cn}r)}{k_{cn}}\, e^{\gamma_n z}\left[B_n^- + \Gamma_n B_n^+\right] \qquad z \le z_1 \tag{20a}$$

$$H_{\phi\mathrm{TM}}(r,z) = j\omega\varepsilon_o\varepsilon_d \sum_{n=1}^{\infty} B_n^+ \frac{S_1(k_{cn}r)}{k_{cn}}\, e^{-\gamma_n z_{sc}} \cdot 2\cosh\gamma_n(z_{sc}-z) \qquad z_2 \le z \le z_{sc} \tag{20b}$$

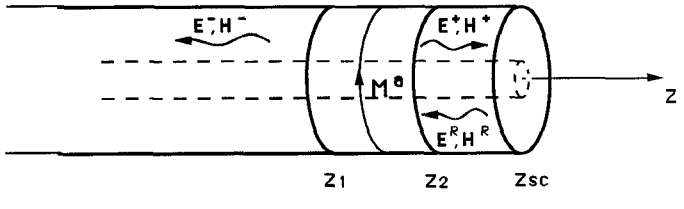

Fig. 4. Geometry for the evaluation of the admittance term Y^a.

where

$$\Gamma_n = e^{-2\gamma_n z_{sc}}$$

$$B_n^\pm = \frac{k_{cn}}{\gamma_n} \frac{r_o S_1(k_{cn}r_o)}{r_o^2 S_1^2(k_{cn}r_o) - r_i^2 S_1^2(k_{cn}r_i)} \cdot V_o \int_{z_1}^{z_2} e^{\pm\gamma_n z} f(z)\, dz$$

$$S_1(k_{cn}r) = J_1(k_{cn}r) - \frac{J_o(k_{cn}r_i)}{N_o(k_{cn}r_i)} N_1(k_{cn}r)$$

$$k_{cn}^2 = \gamma_n^2 + \omega^2\mu_o\varepsilon_o\varepsilon_d\,.$$

The modal expressions are written as a combination of Bessel $(J_n(k_{cn}r))$ and Neumann $(N_n(k_{cn}r))$ functions, and are characterized by eigenvalues k_{cn}, solutions of the transcendental equation

$$J_o(k_{cn}r_i)N_o(k_{cn}r_o) - J_o(k_{cn}r_o)N_o(k_{cn}r_i) = 0\,.$$

Because Lorentz' reciprocity theorem does not give information about the field into the source region, which is, in the present problem, the field to be considered for the evaluation of

$$Y^a = 2\pi r_o \int_{z_1}^{z_2} H_\phi^a(r_o, z', f(z'))\, dz'\,, \tag{21}$$

the source has been divided into two parts, left (L) and right (R), as shown in Fig. (5). In z', the field is the superposition of the two contributions

$$H_\phi^a(r_o, z', f(z')) = \sum_{n=0}^{\infty} H_{\phi n\mathrm{L}}(r_o, z', f(z')) + \sum_{n=0}^{\infty} H_{\phi n\mathrm{R}}(r_o, z', f(z')) \tag{22}$$

where summations include both TEM and TM modes.

The coordinate z' has been introduced to indicate a point inside the source region.

The term due to the left part are obtained by (19b) and (20b), putting $z_2 = z'$ in the limit $z \to z'$; the terms due to the right part are obtained by (19a) and (20a), putting $z_1 = z'$

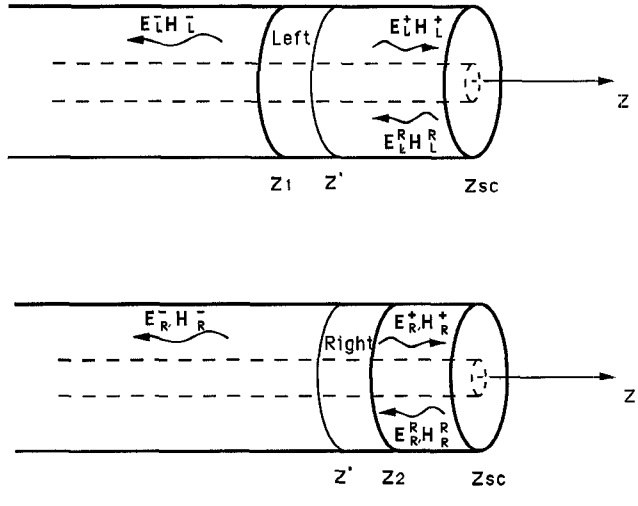

Fig. 5. Evaluation of the field inside the magnetic source region by its subdivision into two contributions.

in the limit $z \to z'$. Computational details are reported in the Appendix.

V. Admittance Term Y^b

The term Y^b represents the load effect of the external medium on the source. The outer region is quite complicated to model because it consists of a half-space ($z \leq 0$), where the magnetic current distribution M_ϕ radiates in the presence of a metallic cylinder (cable external conductor), and half-space ($z > 0$), where the magnetic current distribution M_ϕ radiates into an homogeneous unbounded medium.

To take into account the load effect of the two half-spaces, a reasonable assumption seems to be the subdivision of the source into two equal parts and then the evaluation of the fields in the region $z \leq 0$ by a cylindrical transform representation [27], that implicitly accounts for boundary condition on the conductor, and the fields in the region $z > 0$ by the magnetic current loop field expressions, i.e., for $z \leq 0$,

$$H^b_{\phi<}(r,z) = \frac{1}{4\pi}\int_{-\infty}^{+\infty} \tilde{f}_o(k_z) H_1^{(2)}\left(r\sqrt{k^2-k_z^2}\right) \cdot \sqrt{k^2-k_z^2}\, e^{jk_z z}\, dk_z \tag{23a}$$

where

$$\tilde{f}_o(k_z) = \frac{j\omega\varepsilon_o(\varepsilon' - j\varepsilon'')\tilde{E}_z(k_z)}{(k^2-k_z^2)H_o^{(2)}\left(r_o\sqrt{k^2-k_z^2}\right)}$$

$$\tilde{E}_z(k_z) = \int_{z_1}^{z_2} V_o f(z) e^{-\jmath k_z z}\, dz$$

$H_n^{(2)}$ = Hankel function of second kind and complex argument

$$k^2 = \omega^2\mu_o\varepsilon_o(\varepsilon' - j\varepsilon'')$$

and for $z > 0$,

$$H^b_{\phi>}(r,z) = \frac{1}{\eta_b}\frac{(kr_o)^2 V_o \sin\theta}{8d}\left[1+\frac{1}{jkd}\right]e^{-\jmath kd} \tag{23b}$$

where

$$d = r\sin\theta + z\cos\theta; \qquad \theta = \operatorname{arctg}\frac{r}{z};$$

$$\eta_b = \sqrt{\frac{\mu_o}{\epsilon_o(\epsilon' - j\varepsilon'')}}.$$

In the evaluation of Y^b, it is necessary to calculate the contribution of the two magnetic fields on the source region

$$H^b_\phi(r_o,z) = H^b_{\phi<}(r_o,z) + H^b_{\phi>}(r_o,z) \tag{23c}$$

and then

$$Y^b = 2\pi r_o \int_{z_1}^{z_2} H^b_\phi(r_o,z)\, dz\,. \tag{24}$$

After substituting (23c) in (24), integration along the spatial coordinate z can be easily performed in a closed form, if a proper expansion function is chosen, and integration in the spectral domain is numerically computed.

VI. Expansion Function Choice

In the Method of Moment, the choice of the expansion functions is important because a better accuracy can be achieved with a lower computational effort if the real behavior of the field is taken into account. In the present problem, the most suitable choice should account for the edge condition

$$f(z) = \frac{1}{\sqrt{(z-z_1)(z_2-z)}} \tag{25}$$

but its great disadvantage is that integrations (21) and (24) cannot be performed in a closed form.

In order to simplify the calculation, a constant M has been chosen, and therefore, $f(z)$ also reduces to a constant function whose value is given by (25) evaluated at the center of the radiating gap

$$f(z) = f\left(z = \frac{z_1+z_2}{2}\right) = \frac{2}{z_2-z_1}. \tag{26}$$

Because the evaluation of the field involves integrations of the magnetic current over the aperture, an effective width w_{eff} of the aperture has been adopted together with the choice of (26), such that

$$\int_{z_1}^{z_2} \frac{1}{\sqrt{(z-z_1)(z_2-z)}}\, dz = \frac{2}{z_2-z_1} w_{\text{eff}} \tag{27}$$

and therefore,

$$w_{\text{eff}} = \frac{\pi}{2}(z_2-z_1). \tag{28}$$

In such a way, all expressions involving spatial integration can be evaluated in a closed form.

VII. Reflection Coefficient

Once we evaluate the electric field on the aperture (that is, the value V_o), the modal amplitudes given by (18) are also determined.

In this manner, the input reflection coefficient can be calculated by its definition as the ratio between the backward TEM waves over the incident field. As shown in Fig. 6, it can be expressed by

$$\Gamma_{\text{in}} = \frac{\Gamma_o + C_o^- + \Gamma_o C_o^+}{1} e^{2\jmath\beta z} \qquad z \leq z_1 \tag{29}$$

where Γ_o is the wave due to the incident field of unit amplitude and reflected by the shorted end; C_o^- is the backward TEM wave due to M; and $\Gamma_o C_o^+$ is the forward TEM wave due to M and reflected by the shorted end.

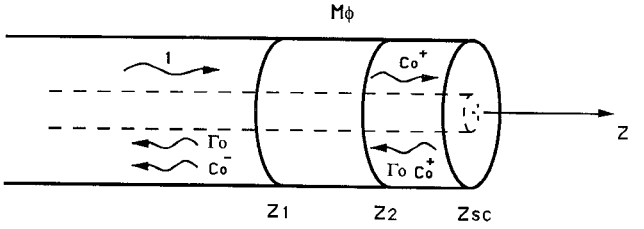

Fig. 6. Forward and backward TEM waves for the reflection coefficient evaluation.

VIII. Radiated Field and Thermic Model

The field radiated by the aperture in a conducting cylinder can be rigorously expressed as

$$E_z(r,\phi,z) = \frac{1}{2\pi j\omega\varepsilon_0(\varepsilon' - j\varepsilon'')} \int_{-\infty}^{\infty} (k^2 - k_z^2) f_o(k_z) \cdot H_o^{(2)}\left(r\sqrt{k^2 - k_z^2}\right) e^{jk_z z}\, dk_z \tag{30a}$$

$$E_\rho(r,\phi,z) = -\frac{1}{2\pi\omega\varepsilon_0(\varepsilon' - j\varepsilon'')} \int_{-\infty}^{\infty} \sqrt{k^2 - k_z^2}\, k_z f_o(k_z) \cdot H_1^{(2)}\left(r\sqrt{k^2 - k_z^2}\right) e^{jk_z z}\, dk_z \tag{30b}$$

where the integrand functions are given in Section V.

In analogy with the model adopted in the above-mentioned section, in the region $z > 0$, the field expression for a magnetic current loop has been used. The power density dissipated in the lossy region is easily obtained by

$$W = \frac{1}{2}\sigma|E|^2 \tag{31}$$

where σ is the conductivity of the lossy medium.

The temperature pattern has been evaluated by solving the bio-heat transfer equation (BHTE)

$$\rho c \frac{\partial T}{\partial t} = \nabla \bullet (k\nabla T) + W + M - B \tag{32}$$

where ρ, c, t, T, k are density, specific heat, time, temperature, and thermic conductivity, respectively; M is the metabolic rate, and B is the heat transfer rate due to local blood flux. The following boundary conditions have been used:

$$\frac{\partial T}{\partial n} = 0 \qquad \text{for regions far from the source}$$

$$k\frac{\partial T}{\partial n} = h(T - T_a) \qquad \text{at the interface between different media}$$

where

n is the direction normal to the boundary

h is the heat transfer coeficient

T_a is a fixed boundary temperature. (34)

The BHTE has been numerically solved using the Hopscotch method [28].

IX. Results

A Sunher UT 85 coaxial cable with the following characteristics has been considered: $2r_o = 1.68$ mm, $2r_i = 0.51$ mm, $Z_o = 50\ \Omega$. The radiating aperture has a width $w = 2$ mm and is placed at the end of the cable ($z_2 = z_{sc}$); the total cable length, including the SMA connector, is 113 mm.

Three different load conditions have been numerically and experimentally investigated: cable embedded in 0.72-molarity and 0.267–molarity NaCl solutions, and cable embedded in a phantom simulating the muscle tissue which exhibits a relative permittivity $\varepsilon' = 47$ and conductivity $\sigma = 2.17$ S/m at $f = 2450$ MHz, and $\varepsilon' = 51$, $\sigma = 1.28$ S/m at $f = 915$ MHz; a linear dependence on the frequency has been adopted in the investigated range of frequency.

In Table I, the theoretical and experimental input impedance is reported for the applicator radiating into the above-mentioned media at three different frequencies. Measurements have been made by a network analyzer HP 8510B, compensating the cable length by an electrical delay of 1.06 ns. The comparison shows that the model can predict the electrical characteristic of the applicator with sufficient accuracy. The low values of the slot impedance indicate that a current maximum occurs at the end of the cable: this is due both to the shorted termination of the cable and to the surrounding high conductive medium; since the slot cuts the flux lines of a high-intensity current, a good efficiency is obtained for the applicator.

In order to test the broadband behavior of the structure, the return loss values are reported in Fig. 7 in the frequency range 2–3 GHz. The differences of ±1 db between theoretical (dots) and experimental (continuous line) values at the lower and upper band limits are probably due to the particular mixture used for the phantom that precisely simulates the muscle complex permittivity at 2450 MHz only. The return loss values (about 6 dB at the work frequency of 2450 MHz) show that the antenna is sufficiently matched to the line for this kind of application.

The thermic behavior of the applicator depends upon the radiated field: the cylindrical transform representation (30a), (30b) intrinsically satisfies the condition of vanishing electric field on the external cable conductor, so the field expressions take into account the effect of the current flowing along the outside of the cable. This current $[I = 2\pi r_o H_\phi^b(r = r_o, z)]$, normalized to the internal incident current wave, is shown in Fig. 8; because of the lossy material surrounding the cable, this current rapidly decays, highlighting that the field is localized close to the radiating slot. This peculiar characteristic is also confirmed by the power density pattern evaluated at different

TABLE I
Theoretical and Experimental Input Impedance

0.267-Molarity NaCl Solution		
Frequency (MHz)	Theoretical	Experimental
2300	$12.25 - j11.2$	$14.3 - j13.4$
2450	$11.61 - j10.9$	$14.5 - j13.6$
2600	$11.1 - j10.57$	$14.54 - j13.4$
0.720-Molarity NaCl Solution		
Frequency (MHz)	Theoretical	Experimental
2300	$13.5 - j6.9$	$15 - j7.3$
2450	$13 - j7$	$15 - j7.7$
2600	$12.4 - j7.1$	$15.1 - j7.66$
Phantom		
Frequency (MHz)	Theoretical	Experimental
2300	$18.8 - j16.3$	$18.2 - j18.5$
2450	$17.9 - j16.2$	$18.3 - j18.4$
2600	$17.1 - j16$	$18.5 - j17.7$

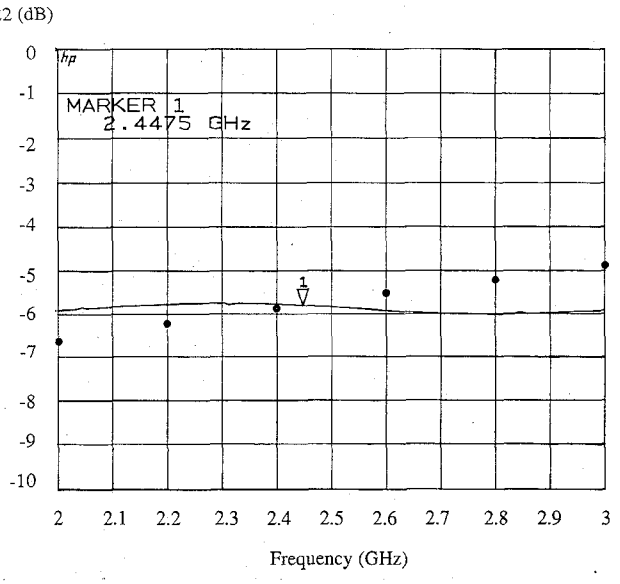

Fig. 7. Experimental (continuous line) and theoretical (dots) return loss values.

distances from the cable surface for an incident power of 1 W, as shown in Fig. 9.

The corresponding temperature pattern after 3 min is reported in Fig. 10 using the following thermic parameters for the phantom: $c = 5000$ J/Kg/°C, $\rho = 950$ Kg/m^3, $k = 0.59$ W/m/°C, steady-state temperature $T = T_a = 22$°C,

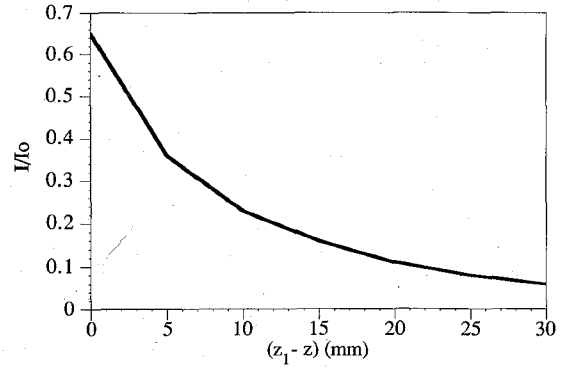

Fig. 8. Current along the external cable conductor, normalized to the internal incident current I_o.

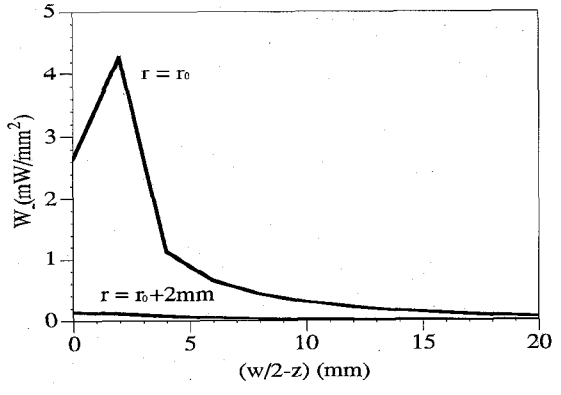

Fig. 9. Power density distribution along z-direction at $r = r_o$ (on the external cable surface) and at $r = r_o + 2$ mm.

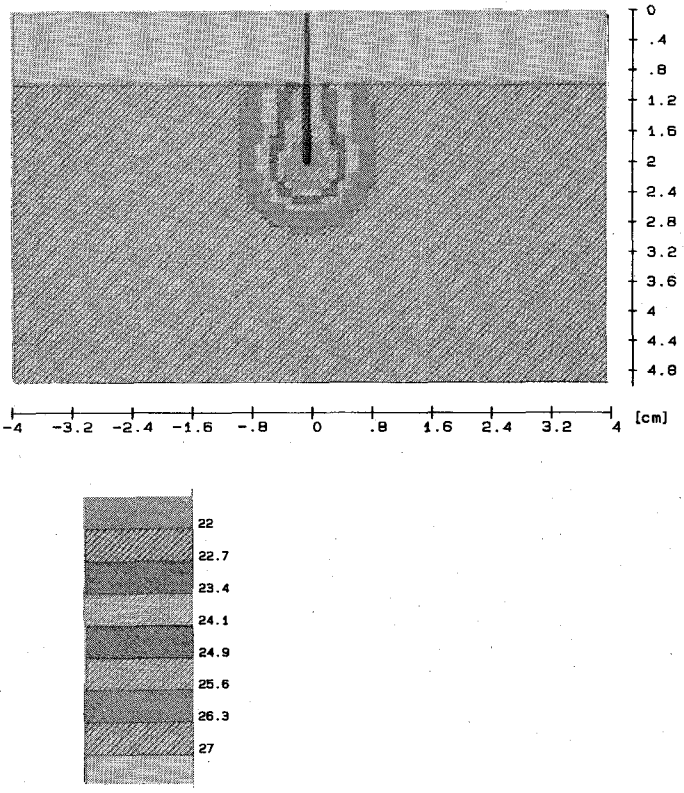

Fig. 10. Simulated temperature pattern.

$h = 14$ W/m^2/°C, $M = B = 0$. A spot of about 2 cm around the tip of the cable has been obtained with a temperature increase of about 4–5°C with respect to the bulk temperature.

Fig. 11 shows the corresponding experimental infrared thermography on the phantom. A satisfactory agreement is achieved as regards spot dimension and temperature increase.

Both the experimental and the theoretical temperature pattern highlights the extension of the heating pattern back along the cable. In the authors' opinion, this is mainly due to two effects. The former effect is the presence of the radial reactive electric field (30b) on the outside of the cable, mainly in the region closer to the slot. The latter effect is due to the high value of the thermic conductivity of the copper, for which heat propagates along the cable more rapidly than in the phantom.

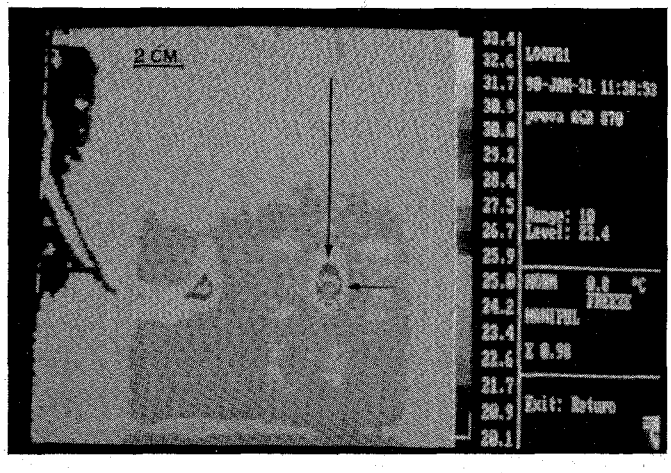

Fig. 11. Infrared thermography temperature pattern.

X. Conclusions

An interstitial applicator has been analyzed; it consists of a shorted coaxial cable with a radiating aperture that provides a temperature enhancement at the tip of the structure.

The application of the equivalence principle leads to an equation for the unknown magnetic current distribution on the aperture; this equation is solved by a simplified form of the Method of Moments.

Results are given in terms of return loss and of temperature pattern; both are compared to experimental data showing a good agreement.

Appendix

After dividing the magnetic source into two partial sources (left "L" and right "R"), each term on the right-hand side of (22) can be expressed as

$$H_{\phi o\mathrm{L}}(r,z') = C^{+}_{o\mathrm{L}}\,\frac{e^{-j\beta z_{cs}}}{r\eta}\,2\cos\beta(z_{sc}-z') \tag{A1}$$

$$H_{\phi n\mathrm{L}}(r,z') = j\omega\varepsilon_o\varepsilon_d \cdot B^{+}_{n\mathrm{L}}\,\frac{S_1(k_{cn}r)}{k_{cn}}\,e^{-\gamma_n z_{sc}}2 \cdot \cosh\gamma_n(z_{sc}-z') \tag{A2}$$

$$H_{\phi o\mathrm{R}}(r,z') = -\frac{e^{j\beta z'}}{r\eta}\left[C^{-}_{o\mathrm{R}} + \Gamma_o C^{+}_{o\mathrm{R}}\right] \tag{A3}$$

$$H_{\phi n\mathrm{R}}(r,z') = j\omega\varepsilon_o\varepsilon_d\,\frac{S_1(k_{cn}r)}{k_{cn}}\,e^{\gamma_n z'} \cdot \left[B^{-}_{nR} + \Gamma_n B^{+}_{nR}\right] \tag{A4}$$

where the subscript "o" is used for the TEM mode and the subscript "n" is used for the TM modes.

In this representation, modal amplitudes $C^{\pm}_o(z')$ and $B^{\pm}_n(z')$ also depend on the partial source extension, and so become a function of z'. Making use of the concept of the effective width w_{eff}, introduced in Section VI, modal amplitudes can be easily evaluated

$$C^{+}_{o\mathrm{L}} = \frac{V_o}{2\ln\left(\frac{r_o}{r_i}\right)}\int_{z_1}^{z'} e^{j\beta z}\,\frac{\pi}{w_{\mathrm{eff}}}\,dz = \frac{V_o\pi\left(e^{j\beta z'} - e^{j\beta z_1}\right)}{j\beta w_{\mathrm{eff}}\,2\ln\left(\frac{r_o}{r_i}\right)} \tag{A5}$$

to be used in (A1)

$$C^{+}_{o\mathrm{R}} = \frac{V_o}{2\ln\left(\frac{r_o}{r_i}\right)}\int_{z'}^{z_2} e^{j\beta z}\,\frac{\pi}{w_{\mathrm{eff}}}\,dz = \frac{V_o\pi\left(e^{j\beta z_2} - e^{j\beta z'}\right)}{j\beta w_{\mathrm{eff}}\,2\ln\left(\frac{r_o}{r_i}\right)} \tag{A6}$$

$$C^{-}_{o\mathrm{R}} = -\frac{V_o}{2\ln\left(\frac{r_o}{r_i}\right)}\int_{z'}^{z_2} e^{-j\beta z}\,\frac{\pi}{w_{\mathrm{eff}}}\,dz = \frac{V_o\pi\left(e^{-j\beta z_2} - e^{-j\beta z'}\right)}{j\beta w_{\mathrm{eff}}\,2\ln\left(\frac{r_o}{r_i}\right)} \tag{A7}$$

to be used in (A3); and similarly,

$$B^{+}_{n\mathrm{L}} = \frac{V_o k_{cn}\pi r_o S_1(k_{cn}r_o)\left[e^{\gamma_n z'} - e^{\gamma_n z_1}\right]}{\gamma_n^2[r_o^2 S_1^2(k_{cn}r_o) - r_i^2 S_1^2(k_{cn}r_i)]w_{\mathrm{eff}}} \tag{A8}$$

to be used in (A2)

$$B^{+}_{n\mathrm{R}} = \frac{V_o k_{cn}\pi r_o S_1(k_{cn}r_o)\left[e^{\gamma_n z_2} - e^{\gamma_n z'}\right]}{\gamma_n^2[r_o^2 S_1^2(k_{cn}r_o) - r_i^2 S_1^2(k_{cn}r_i)]w_{\mathrm{eff}}} \tag{A9}$$

$$B^{-}_{n\mathrm{R}} = -\frac{V_o k_{cn}\pi r_o S_1(k_{cn}r_o)\left[e^{-\gamma_n z_2} - e^{-\gamma_n z'}\right]}{\gamma_n^2[r_o^2 S_1^2(k_{cn}r_o) - r_i^2 S_1^2(k_{cn}r_i)]w_{\mathrm{eff}}} \tag{A10}$$

to be used in (A4).

In such a way, each term of (22) is defined and can be substituted in (21) to determine Y^a in a closed form. In the examinated case, where the slot is placed at the end of the cable ($z_{sc} = z_2 = 0$), the admittance Y^a assumes the value

$$Y^a = -\frac{j2V_o\pi\left[1 - e^{-j\beta w_{\mathrm{eff}}}\cdot\frac{\sin(\beta w_{\mathrm{err}})}{\beta w_{\mathrm{eff}}}\right]}{\omega\mu_o\ln\left(\frac{r_o}{r_i}\right)} + j2\omega\varepsilon_o\varepsilon_d V_o\pi\sum_{n=1}^{\infty} \cdot \frac{r_o^2 S_1^2(k_{cn}r_o)\left[2 + \frac{e^{-2\gamma_n w_{\mathrm{eff}}}-1}{\gamma_n w_{\mathrm{eff}}}\right]}{\gamma_n^2[r_0^2 S_1^2(k_{cn}r_o) + r_i^2 S_1^2(k_{cn}r_i)]}. \tag{A11}$$

References

[1] B. Enami, C. A. Perez, L. Leybovich, W. Straube, and D. Vongerichten, "Interstitial thermoradiotherapy in treatment of malignant tumors," *Int. J. Hyperthermia,* vol. 3, no. 2, pp. 107–118, 1987.

[2] P. R. Stauffer, P. K. Sneed, S. A. Suen, T. Satoh, K. Matsumoto, J. R. Fike, and T. L. Phillips, "Comparative thermal dosimetry of interstitial microwave and radiofrequency-LCF hyperthermia," *Int. J. Hyperthermia,* vol. 5, no. 3, pp. 307–318, 1989.

[3] L. S. Taylor, "Devices for microwave hyperthermia," in *Cancer Therapy by Hyperthermia and Radiation,* X. Streffer, Ed. Munich: Verlag Urban & Schwarzenberg, 1978, pp. 115–117.

[4] C. Marchal, M. Nadi, S. Hoffstetter, P. Bey, M. Pernot, and G. Prieur, "Practical interstitial method of heating operating at 27.12 MHz," *Int. J. Hyperthermia,* vol. 5, no. 4, pp. 451–466, 1989.

[5] A. G. Visser, I. K. K. Deurloo, P. C. Levendag, A. C. C. Ruifrok, B. Cornet, and G. C. Van Rhoon, "An interstitial hyperthermia system at 27 MHz," *Int. J. Hyperthermia,* vol. 5, no. 2, pp. 265–276, 1989.

[6] J. M. Cosset, J. Dutreix, C. Haie, A. Gerbaulet, P. Janoray, and J. A. Dewar, "Interstitial thermoradiotherapy: A technical and clinical study of 29 implantations performed at the Institut Gustave-Roussy," *Int. J. Hyperthermia,* vol. 1, no. 1, pp. 3–13, 1985.

[7] M. A. Astrahan, G. Luxton, M. D. Sapozink, and Z. Petrovich, "The accuracy of temperature measurement from within an interstitial microwave antenna," *Int. J. Hyperthermia,* vol. 4, no. 6, pp. 693–607, 1988.

[8] R. W. P. King, S. R. Mishra, K. M. Lee, and G. S. Smith, "The insulated monopole: Admittance and junction effects," *IEEE Trans. Antennas Propagat.,* vol. AP-23, pp. 172–177, Mar. 1975.

[9] R. W. P. King, B. S. Trembly, and J. W. Strohbehn, "The electromagnetic field of an isolated antenna in a conducting or dielectric medium," *IEEE Trans. Microwave Theory Tech.,* vol. MTT-31, pp. 574–583, July 1983.

[10] J. P. Casey and R. Bansal, "The near field of an insulated dipole in a dissipative dielectric medium," *IEEE Trans. Microwave Theory Tech.,* vol. MTT-34, pp. 459–463, Apr. 1986.

[11] M. F. Iskander and A. M. Tumeh, "Design optimization of interstitial antennas," *IEEE Trans. Biomed. Eng.,* vol. 36, pp. 238–246, Feb. 1989.

[12] W. Hurter, F. Reinbold, and W. J. Lorenz, "A dipole antenna for interstitial microwave hyperthermia," *IEEE Trans. Microwave Theory Tech.,* vol. MTT-39, pp. 1048–1054, June 1991.

[13] V. Eppert, B. S. Trembly, and H. J. Richter, "Air cooling for an interstitial microwave hyperthermia antenna: Theory and experiment," *IEEE Trans. Biomed. Eng.,* vol. 38, pp. 450–460, May 1991.
[14] A. M. Tumeh and M. F. Iskander, "Performance comparison of available interstitial antennas for microwave hyperthermia," *IEEE Trans. Microwave Theory Tech.,* vol. MTT-37, pp. 1126–1133, July 1989.
[15] K. M. Jones, J. A. Mechling, B. S. Trembly, and J. W. Stohbehn, "SAR distributions for 915 MHz interstitial microwave antennas used in hyperthermia for cancer therapy," *IEEE Trans. Biomed. Eng.,* vol. 35, pp. 851–857, Oct. 1988.
[16] B. S. Trembly, "The effects of driving frequency and antenna length on power deposition within a microwave antenna array used for hyperthermia," *IEEE Trans. Biomed. Eng.,* vol. 32, pp. 152–157, Feb. 1985.
[17] C. M. Furse and M. F. Iskander, "Three-dimensional electromagnetic power deposition in tumors using interstitial antenna arrays," *IEEE Trans. Biomed. Eng.,* vol. 36, pp. 977–986, Oct. 1989.
[18] Y. Zhang, W. T. Joines, and J. R. Oleson, "The calculated and measured temperature distribution of phased interstitial antenna array," *IEEE Trans. Microwave Theory Tech.,* vol. MTT-38, pp. 69–77, Jan. 1990.
[19] P. F. Turner, "Interstitial equal-phased arrays for EM hyperthermia," *IEEE Trans. Microwave Theory Tech.,* vol. MTT-34, pp. 572–578, May 1986.
[20] B. S. Trembly, A. H. Wilson, M. J. Sullivan, A. D. Stein, T. Z. Wong, and J. W. Stohbehn, "Control of the SAR pattern within an interstitial microwave array through variation of antenna driving phase," *IEEE Trans. Microwave Theory Tech.,* vol. MTT-34, pp. 568–571, May 1986.
[21] T. Z. Wong, J. W. Strohbehn, K. M. Jones, J. A. Mechling, and B. S. Trembly, "SAR patterns from interstitial microwave antenna-array hyperthermia system," *IEEE Trans. Microwave Theory Tech.,* vol. MTT-34, pp. 560–567, May 1986.
[22] J. C. Lin and Y.-J. Wang, "Interstitial microwave antennas for thermal therapy," *Int. J. Hyperthermia,* vol. 3, no. 1, pp. 37–47, 1987.
[23] ——, "An implantable microwave antenna for interstitial hyperthermia," *Proc. IEEE,* vol. 75, pp. 1132–1133, Aug. 1987.
[24] J. C. Lin, "Biomedical uses of electromagnetic technology," in *Proc. 9th Int. Zurich Symp. Electromagnetic Compatibility,* Zurich, Switzerland, Mar. 12–14, 1991, pp. 323–328.
[25] G. Cerri, R. De Leo, and V. Mariani Primiani, "Interstitial end-fire applicators: Analysis and experimental results," in *Proc. 21th Euro. Microwave Conf.,* Stuttgart, Germany, Sept. 9–12, 1991, pp. 1427–1432.
[26] R. F. Harrington, *Field computation by Moment Method.* New York: Macmillan, 1968.
[27] ——, Time–Harmonic Electromagnetic Fields. New York: McGraw-Hill, 1961.
[28] A. R. Gourlay, "Hopscotch: A fast second-order partial differential equation solver," *J. Inst. Math. Appl.,* no. 6, pp. 375–390, 1970.

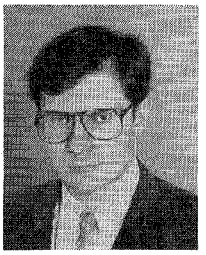

Graziano Cerri was born in Ancona, Italy, in 1956. He received the degree in electronic engineering from the University of Ancona in 1981.

Since 1983 he has been with the Department of Electronics and Automatics at the University of Ancona as a researcher. His research is mainly devoted to microstrip antennas and hyperthermia. Currently he is also involved in EMC problems and in the analysis of the interaction between EM fields and biological bodies.

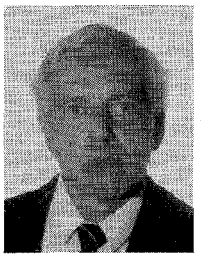

Roberto De Leo was born in Bari, Italy, in 1942. He graduated from the Politecnico di Torino, Italy, in 1965.

From 1966 to 1980 he was at the University of Bari, working on microwave devices. Since 1980 he has been a Full Professor of Electromagnetics at the University of Ancona, Italy. His areas of interest are medical applications of electromagnetic waves and electromagnetic compatibility.

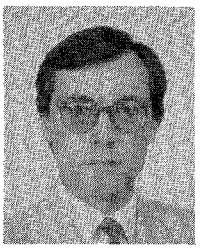

Valter Mariani Primiani was born in Rome, Italy, in 1961. He received the degree in electronic engineering from the University of Ancona, Italy, in 1990.

Since 1981 he has been a Laboratory Researcher at the University of Ancona. His area of interest concerns microwave path antennas, medical applications of electromagnetic waves, and electromagnetic compatibility.